Composites Science and Technology 68 (2008) 1624–1630

Contents lists available at ScienceDirect

Composites Science and Technology

journal homepage: www.elsevier.com/locate/compscitech

Woven fabric permeability: From textile deformation to fluid flow mesoscale simulations

F. Loix [a], P. Badel [b], L. Orgéas [a,*], C. Geindreau [a], P. Boisse [b]

[a] Laboratoire Sols-Solides-Structures-Risques (3SR), CNRS – Université de Grenoble (INPG-UJF), BP 53, 38041 Grenoble Cedex 9, France
[b] Laboratoire de Mécanique des Contacts et des Structures (LaMCoS), CNRS – INSA Lyon, Bâtiment Jacquard, Rue Jean Capelle, F69621 Villeurbanne Cedex, France

ARTICLE INFO

Article history:
Received 5 September 2007
Received in revised form 15 February 2008
Accepted 19 February 2008
Available online 5 March 2008

Keywords:
A. Fabrics/textiles
B. Shear deformation
B. Permeability
C. Finite element analysis (FEA)
E. Multiscale modelling

ABSTRACT

A two-step methodology is proposed in order to estimate from numerical simulations the permeability of deformed woven fabrics. Firstly, the shear deformation of a glass plain weave until the shear locking is studied from a mesoscale analysis achieved with a representative volume element (RVE) of the periodic plain weave. Simulations have been carried out within the scope of large transformations, accounting for yarn–yarn contacts, and assuming that yarns behave as hypoelastic materials with transverse isotropy. From the simulated deformed solid RVE, a complementary periodic fluid RVE is then built and the slow flow of an incompressible Newtonian fluid within it is investigated. This allows to compute, in a second step, the permeability of the deformed plain weave. The role of the shear deformation on the permeability of multi-layers or single layer preforms is discussed.

1. Introduction

It is essential to accurately predict flows in fibre preforms for a number of liquid molding processes among which the resin transfer moulding process (RTM). Nevertheless, the determination with a high precision of the permeability, which is one of the most important parameter influencing those flows, still remains difficult. Woven fabrics' manufacturers can provide a material property list which sometimes contains the permeability of fabrics, usually measured when fabrics are not deformed. However, during the preforming stage of RTM woven fabrics undergo mechanical loadings which can induce very large deformations of the textiles of which dominant mode is the shear deformation [1]. This can strongly affect their permeability and has to be understood and quantified. Indeed, the relation between deformation and permeability being determined and the deformation pattern of the fabrics being known, the related permeability pattern can be drawn for the entire reinforcement in order to better predict the flow within the preform [2].

A possible way to circumvent the above difficulty is to perform numerical simulations in order to predict the permeability of a deformed fibre reinforcement. For that purpose, two steps have to be performed. The first step consists in modelling the pre-deformation of the dry woven textile, taking into account mechanical properties of the yarns as well as their interactions. The second step consists in simulating the flow of the polymer resin through the as-deformed textile in order to compute the permeability. Within such a framework, 2D simplified permeability models which have been validated with experimental measurements have already been developed [3–8]. These studies showed the significant influence of shear on principal permeabilities of reinforcements. Some of them [3,5–7] also highlighted two relevant factors when considering experimental flows in sheared fabrics, i.e. the ratio of principal permeabilities and the direction of principal axes of the permeability tensor with respect to the shear deformation of the fibre reinforcement. When the shear angle is below the locking angle of the woven fabric, rather good agreement is generally observed between the permeability model prediction and measurements [8]. 3D models of the permeability have also been developed [9–13]. Simacek and Advani [9] and Dungan et al. [10] highlighted the influence of the number of layers and of the nesting effect on the permeability. A decrease of the in-plane permeability with the number of layers was indeed shown [10]. Nevertheless, no detail is brought on the mechanical model used to describe the 3D pre-deformation of the dry reinforcement in [9–11]. Finally, Laine et al. [12,13] investigated two ways to construct the fluid volume around the deformed textile. The first consists in using "voxelization" of a real representative volume element (RVE) obtained from X-ray microtomography. In that case,

* Corresponding author. Tel.: +33 4 76 82 70 73; fax: +33 4 76 82 70 43.
E-mail address: laurent.orgeas@hmg.inpg.fr (L. Orgéas).

0266-3538/$ - see front matter © 2008 Elsevier Ltd. All rights reserved.
doi:10.1016/j.compscitech.2008.02.027

the geometry description of the real medium depends on the equipment resolution. This can sometimes be a limiting factor. The second way investigated is to use two software's (Wisetex [14] and the consistent modelling developed in [15]) to generate the solid geometry, to induce the mechanical deformation, to build the fluid volume and then study the fluid flow on that latter volume. Nevertheless, for the construction of the fluid volume, as mentioned the authors, it is crucial to work with a consistent model for the yarn assembly.

Hence to our knowledge, in none of those numerical studies the pre-deformation of textiles is computed taking into account (i) the complex mechanical behaviour of the yarns made of several thousands of fibres, (ii) the inter-yarn contacts and (iii) appropriate periodic boundary conditions. On the other hand, none of the above studies offer a way to compute the permeability tensor as based on a consistent mesoscale model of the 3D deformation of woven fabrics *and* on a 3D meso–macro model for the fluid flow through them. Within that context, the aim of this contribution is to develop a complete methodology allowing to determine numerically the permeability when considering slow saturated flows through woven fabrics that have been previously deformed. For that purpose, a numerical mesoscale model of the shear deformation of a typical plain weave fabric is firstly developed in Section 2. Such a model accounts for the complex anisotropic and compressible mechanical behaviour of the yarns, yarn–yarn contacts, as well as large geometrical transformations induced during the preforming stage. Section 3 is devoted to the determination of permeability of the as-deformed woven fabrics. It is firstly explicated how fluid RVE's can be obtained from deformed solid RVE's. Therefrom, mesoscale numerical simulations are performed with fluid RVE's in order to compute the corresponding permeabilities. Influences of the shear angle and the differences between a single and a multi-layers configurations are then analysed.

2. Mesoscale model of the shear deformation of textiles

The 3D Finite Element (FE) analysis presented in this section has been achieved with the FE code Abaqus. It has two distinct objectives. One of them consists in determining the equivalent macroscopic mechanical behaviour of the textile reinforcement from mesoscale simulations of its deformation under mechanical loadings (here in-plane shear). These properties can then be used in macroscale simulations of the woven reinforcement forming [16]. The other one, of interest in this paper, is to provide local mesoscopic results, namely the deformed geometry of a solid RVE of the considered textile. It will be used in the next section as geometric data for the fluid flow simulations.

Such an analysis presents several delicate aspects to deal with. Firstly, industrial textiles may be subjected to very high shear angles, so that the analysis must be achieved within the scope of large geometrical transformations. Secondly, woven fabrics display periodic (or quasi-periodic) microstructures that are made of several independent yarns. Hence, a particular attention must be paid in order to use and deform consistent microstructures and impose them appropriate periodic boundary conditions (Section 2.1). Lastly, suitable constitutive equations must be used in order to model the mechanical behaviour of yarns (Section 2.2).

2.1. Geometrical model and periodic boundary conditions

The considered woven fabric is sketched in Fig. 1a. It is a glass plain weave which is balanced since the warp and the weft yarns have identical geometrical and mechanical properties. The geometry of the model is based on circle arcs and tangent segments (see Fig. 2). It is simple but ensures consistency of the model, which means that yarns do not penetrate each other [15]. Any pattern allowing to construct the woven reinforcement by translations can be chosen as a representative solid volume. One of the smallest ones, i.e. RVE's, is chosen, for instance the solid RVE depicted in Fig. 1b. It exhibits entirely material boundaries, which lets us prescribe periodic conditions in a classical manner over the domain's boundary [17]. To this end, the displacement field is split into a macroscopic average part (the shear field) and a local periodic fluctuation part, which leads to defining kinematical boundary conditions for each material point of the boundaries. More details about other requirements can be found in [17].

2.2. Constitutive equations of a yarn at finite strains

A yarn of a woven reinforcement is made of several thousands of parallel fibres. In the present mesoscopic FE analysis, it will be considered as a continuum because there are too many fibres. Moreover, rate constitutive equations, also known as hypoelastic laws are used to model its mechanical behaviour. This type of equations is widely used in FE codes [18,19]

$$\underline{\underline{\sigma}}^{\nabla} = \underline{\underline{\underline{\underline{C}}}} : \underline{\underline{D}}, \tag{1}$$

where $\underline{\underline{\sigma}}$ and $\underline{\underline{D}}$ stand respectively for the Cauchy stress tensor and the strain rate tensor and where the fourth order tensor $\underline{\underline{\underline{\underline{C}}}}$ is the tangent stiffness tensor. It is here assumed that the yarn displays transverse isotropy which the local direction follows the direction of the

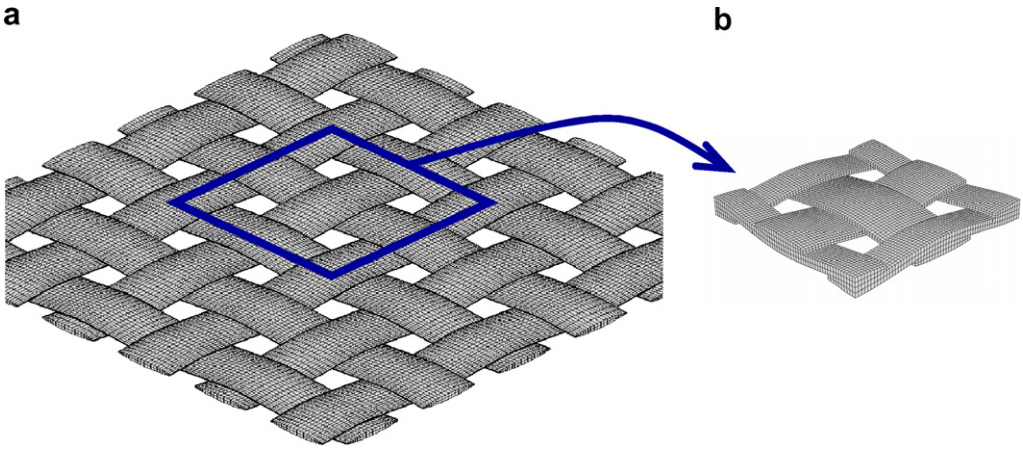

Fig. 1. Scheme of the glass plain weave fabric considered in this work (a) and associated solid RVE (b) with its finite element mesh used to run the simulations.

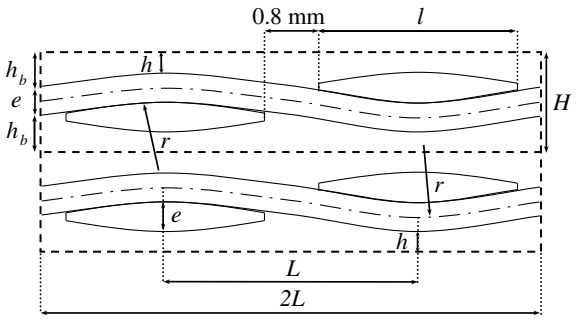

Fig. 2. Sketch of two superimposed fluid RVE's and their corresponding dimensions in the non-deformed configuration. Curvature radius $r = 9.82$ mm, yarn width $l = 3.2$ mm, length of the fluid RVE $2L = 8$ mm, yarn thickness $e = 0.37$ mm, air-gap between layers $2h$, air-gap on the lateral boundaries $2h_b$ and fluid RVE thickness H. When $h = 0$ mm, then $h_b \approx 0.18$ mm and $H \approx 0.74$ mm. The dashed lines represent the boundaries of the fluid RVE.

fibres and is characterised by a unit vector noted $\underline{F}_1$ and $\underline{f}_1$ in the initial and deformed configurations, respectively. Hence, $\underline{\underline{C}}$ only requires five constitutive parameters: longitudinal Young modulus E_1 and Poisson ratio ν_1, transverse Young modulus E_t and Poisson ratio ν_t and a shear modulus G.

It is important to notice that $\underline{\underline{\sigma}}^{\nabla}$ involved in (1) represents the objective derivative of the Cauchy stress tensor $\underline{\underline{\sigma}}$. The aim of this derivative is to avoid undesirable rigid body contributions in the time derivative $\mathrm{d}\underline{\underline{\sigma}}/\mathrm{d}t$. An objective derivative can be considered as a derivative for an observer who is fixed with respect to the material. Several objective rates exist but considering the implementation in a FE code, the simplest ones are the rotational rates

$$\underline{\underline{\sigma}}^{\nabla} = \underline{\underline{Q}} \cdot \left(\frac{\mathrm{d}}{\mathrm{d}t} (\underline{\underline{Q}}^{\mathrm{T}} \cdot \underline{\underline{\sigma}} \cdot \underline{\underline{Q}}) \right) \cdot \underline{\underline{Q}}^{\mathrm{T}}, \tag{2}$$

where $\underline{\underline{Q}}$ is a rotation tensor close to the rotation of the material. It defines the so-called "rotated frame". The application to fibrous materials requires that $\underline{\underline{Q}}$ and the rotated frame are, respectively, the rotation of the fibres and its associated basis $\{\underline{f}_1, \underline{f}_2, \underline{f}_3\}$. Indeed, the longitudinal stiffness of a yarn is usually much larger than the transverse one. As a consequence, the longitudinal direction of the yarn must be accurately tracked because a small angle variation would cause a large stress variation. Therefore the rotation to be used for a bundle of parallel fibres is the rotation which follows the longitudinal direction of the fibres $\underline{f}_1$. To determine $\underline{\underline{Q}}$, the gradient of the geometrical transformation $\underline{\underline{F}}$ is used. Since the initial fibres' direction $\underline{F}_1$ is a material direction, it is transformed by $\underline{\underline{F}}$ into $\underline{f}_1$ as $\underline{f}_1 = \underline{\underline{F}} \cdot \underline{F}_1 / \|\underline{\underline{F}} \cdot \underline{F}_1\|$. The two other initial transverse unit vectors $\underline{F}_2$ and $\underline{F}_3$ are chosen arbitrarily since we assume transverse isotropy. In order to form the orthogonal basis $\{\underline{f}_1, \underline{f}_2, \underline{f}_3\}$in the current configuration, $\underline{f}_2$ and $\underline{f}_3$ are determined with the following expressions:

$$\underline{f}_2 = \frac{\underline{\underline{F}} \cdot \underline{F}_2 - (\underline{f}_1 \cdot \underline{\underline{F}} \cdot \underline{F}_2)\underline{f}_1}{\|\underline{\underline{F}} \cdot \underline{F}_2 - (\underline{f}_1 \cdot \underline{\underline{F}} \cdot \underline{F}_2)\underline{f}_1\|}, \quad \underline{f}_3 = \underline{f}_1 \times \underline{f}_2. \tag{3}$$

Therewith, the rotation can be computed as $\underline{\underline{Q}} = \underline{f}_i \otimes \underline{F}_i$. Eventually, to implement the incremental form of (1), the aim is to compute $\underline{\underline{\sigma}}^{n+1}$ knowing $\underline{\underline{\sigma}}^{n}$, the displacement field at t^{n+1} and the time increment Δt. Writing all of the quantities in the basis $\{\underline{f}_i\}$ and integrating (1) over the time increment Δt, one obtains the stress update formula of Hughes and Winget [18]

$$[\sigma^{n+1}]_{\underline{f}_i^{n+1}} = [\sigma^{n}]_{\underline{f}_j^{n}} + [C^{n+1/2}]_{\underline{f}_j^{n+1/2}} [D^{n+1/2}]_{\underline{f}_i^{n+1/2}} \Delta t, \tag{4}$$

where $[\sigma^n]_{\underline{f}_i^n}$ denotes the matrix of the components of the tensor $\underline{\underline{\sigma}}^n$ in the basis $\{\underline{f}_i\}$ which is the calculation basis defined above.

Previous developments have been intended to deal with the very high longitudinal stiffness the yarn. The second aspect to be focused on is the transverse behaviour of the yarn. This will be very important since the yarn deformation highly depends on it. Two physical phenomena have to be included in the constitutive model. If the yarn undergoes longitudinal tension, it becomes transversely much stiffer. In addition, under transverse compaction, the fibre network densifies so that the transverse stiffness of the equivalent continuum has to increase accordingly. The following model is used: $E_t(c, \varepsilon_{11}) = E_0 + k|\varepsilon_{11}|c^2$, where c is a measure of the transverse compaction, namely the local cross section area variation computed from $\underline{\underline{F}}$, and ε_{11} is the longitudinal strain in the $\underline{f}_1$ direction. E_0 and k are two parameters that have been fitted – via an inverse method – on a biaxial tension experimental test because this test leads to a significant transverse compaction of the yarns [20].

2.3. Examples of results

Fig. 3 shows the evolution of the computed macroscopic shear torque as function of the imposed macroscopic shear angle, when deforming the considered plain weave textile [17]. Fig. 4a–c shows the corresponding solid RVE at three imposed shear angles, *i.e.* 0°, 28° and 53°, respectively. To run the simulation [17], constitutive parameters E_1, E_0, k, ν_1, ν_t, and G have been set to 35400 MPa, 4 MPa, 2.5×10^{-5} MPa, 0, 0 and 10 MPa, respectively. Moreover, the consistent yarn–yarn contact were assumed to induce Coulombic dry friction forces with a friction coefficient $f = 0.2$. Notice that at a shear angle of 53°, i.e. at the end of the transformation, the RVE exhibits shear locking. One can also notice in Fig. 3 the sharp increase of the shear stiffness above 30°, which is related to the lateral crushing of the yarns as the in-plane square RVE geometry turns into a rhombus one. The experimental test referred to consists of a picture frame device. The initially square picture frame moves into a rhomboid, thus the specimen within the frame is subjected to a pure shear strain field. This figure also shows that the agreement between experiment and numerical simulation is rather good [17], keeping in mind (i) that the transverse behaviour of the yarn mechanical model plays a leading role on numerical results, (ii) that spurious tensions are very difficult to avoid in the used picture frame experiment, tending to slightly overestimate the experimental shear curve at large shear angles (this is the reason why experiments may be different from one test to another [21]).

Presently, only a qualitative validation of the deformed result is possible. The deformed geometry of the solid RVE and of each yarn is consistent with what one can expect and observe on a deformed fabric. Besides, no penetration occurs, which is important for the

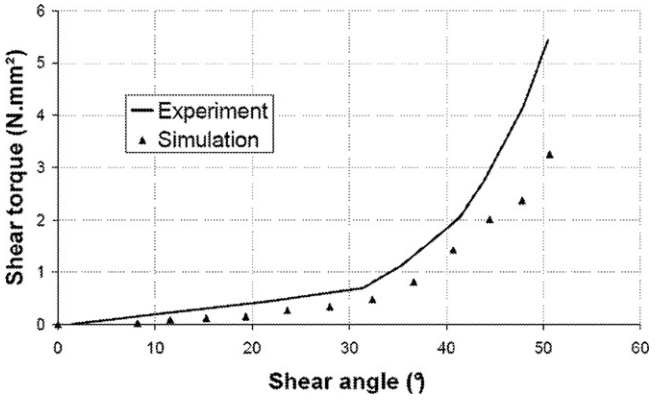

Fig. 3. Evolution of the macroscopic shear torque as a function of the imposed macroscopic shear angle recorded during the shear deformation of the glass plain weave fabric: comparison between experimental and numerical results.

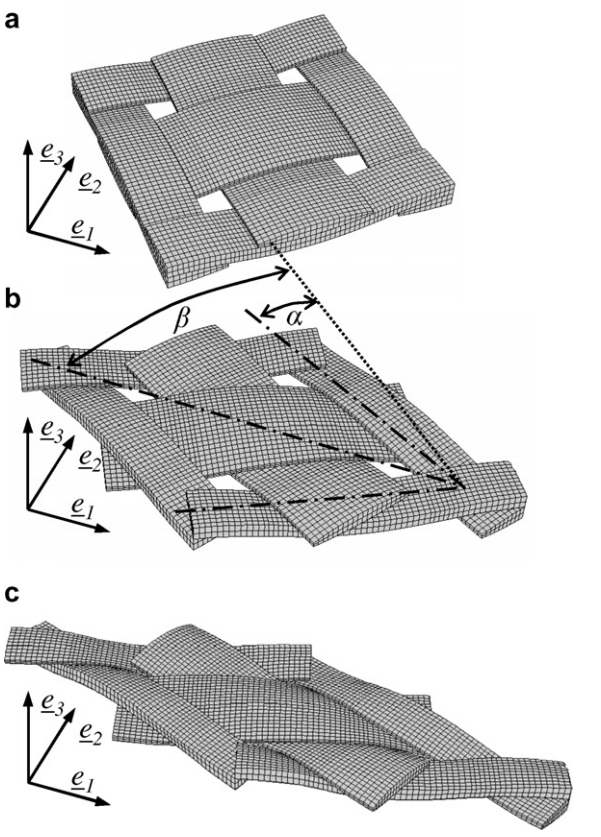

Fig. 4. Solid RVE's for the non-deformed configuration (a) and for shear angles of 28° (b) and 53° (c). Shear angle α and angle of principal direction β are defined in (b).

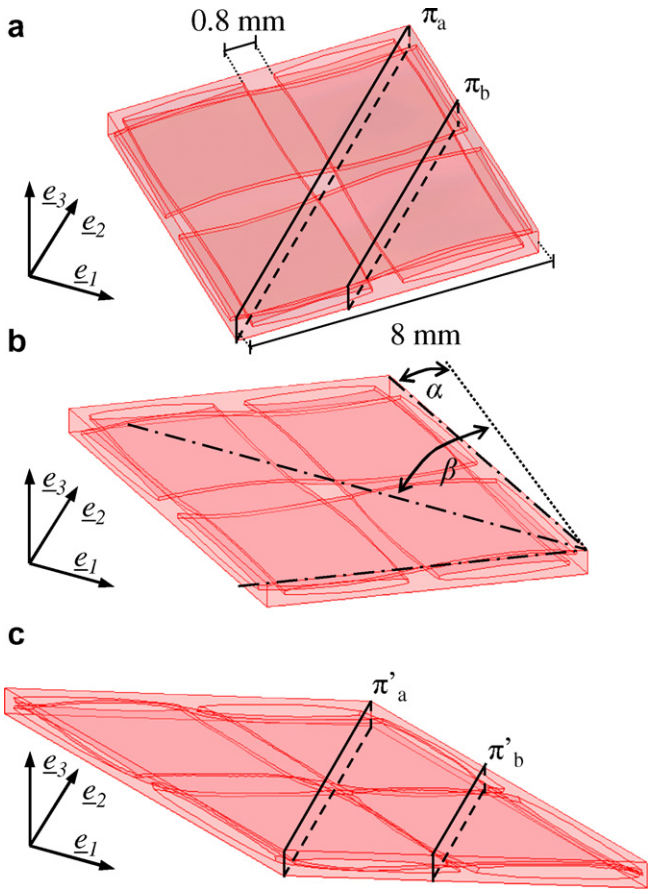

Fig. 5. Fluid RVE's for the non-deformed configuration (a) and for shear angles of 28° (b) and 53° (c). Slice planes π and π' used for colour maps given in Fig. 7 are defined in (a). Shear angle α and angle of principal direction β are defined in (b).

following steps. A quantitative validation of the deformed geometry is in progress using 3D micro tomography to get more accurate information about local deformation of yarns.

3. Meso–macro model for the permeability of deformed textiles

3.1. Determination of the fluid RVE

The present issue is to compute the fluid volume in an appropriate numerical format, the deformed solid geometry being here considered as a given data. Whereas at a first glance that question may seem very simple, it reveals to be not so straightforward for the fibrous microstructure under consideration and to ask for paying long time and large attention. The main problems encountered at this stage are related to CAD issues. Indeed, results obtained with Abaqus are represented by means of meshes for each individual yarn. Those meshes have first to be transformed into solid entities which must then be assembled together to form a unique solid. Those operations are very sensitive and some manual fittings are sometimes needed. Once the unique solid entity is obtained, it is subtracted from a well-chosen volume to give the fluid RVE. As shown in Fig. 4, it appears that it is difficult to construct a fluid RVE as based on the same period as the solid RVE. Instead, a rhombus-shape period was preferred because it circumvents the latter problem, allowing moreover to impose appropriate periodic boundary conditions in a straight way. As examples, fluid RVE's corresponding to the solid REV's depicted in Fig. 4 are represented in Fig. 5 for different imposed shear deformations of the woven fabric and for a chosen vanished air-gap, which is defined as the minimum distance '2h' between the yarn and the fluid RVE boundaries in the $\underline{e}_3$ direction (see Fig. 2). In this context, the thickness of the boxes reveals to be the same and is fixed at 0.74 mm while the porosity ϕ, defined as the ratio between the fluid volume and the total RVE volume, varies with the shear angle, being equal to 0.382, 0.389, 0.403, 0.387 and 0.352 when the shear angle is 0°, 14°, 28°, 41° and 53°, respectively. Let us finally note that the yarn permeability is here considered as being at least two order of magnitude smaller than the woven fabrics permeability. Thus, flows inside individual yarns is neglected [22,23] and the 3D volume of interest remains the volume between the deformed yarn assembly, i.e. the so-called mesopores.

3.2. Method to compute the permeability

Once the fluid volume is obtained, a local fluid flow problem must be solved in this domain in order to compute the macroscopic flow law. In this study, the isothermal slow flow of an incompressible Newtonian fluid of constant viscosity η is considered, for a sake of simplicity. Moreover the domain is supposed to be saturated by the fluid so that there is no capillarity effect. Likewise, the problem is studied within the scope proposed by the homogenisation method with multiple scale asymptotic expansions [24–26]. Under such hypotheses, it can be shown that the macroscopic description is the linear Darcy's law

$$\langle \underline{v} \rangle = -\frac{1}{\eta} \underline{\underline{K}} \cdot \nabla \bar{p}, \tag{5}$$

where $\langle \underline{v} \rangle$ stands for the volume average of the velocity field in the fluid RVE's, $\nabla \bar{p}$ for the macroscopic pressure gradient and $\underline{\underline{K}}$ for the permeability tensor which depends on the microscopic features of

the considered porous media. $\underline{\underline{K}}$ can be obtained from numerical simulation by solving over the periodic fluid RVE's sketched in Fig. 5 the following boundary value problem arising from the homogenisation process [24] (the fluid RVE being denoted by Ω_f, its interior boundaries by $\partial\Omega_f^i$ and its exterior boundaries by $\partial\Omega_f^e$)

$$\begin{cases} 0 = \underline{\nabla} \cdot \underline{v} & \text{on } \Omega_f \text{ (mass conservation)}, \\ 0 = \eta \Delta \underline{v} - \underline{\nabla}\bar{p} - \underline{\nabla}\delta p & \text{on } \Omega_f \text{ (momentum conservation)}, \\ \underline{v} = \underline{0} & \text{on } \partial\Omega_f^i \text{ (no slip boundary conditions)}, \\ \text{Periodic boundary conditions for } \underline{v} \text{ and } \delta p \text{ on } \partial\Omega_f^e, \end{cases} \tag{6}$$

where $\underline{v}$ here stands for the microscopic velocity field, the macroscopic pressure gradient $\underline{\nabla}\bar{p}$ acts as a constant and given volume force in the whole RVE and δp is the first order periodic fluctuation of the pressure around $\bar{p}$. The above equations show that the fluid flow is driven by a balance between local volumetric viscous drag forces of characteristic value $f_c = \eta v_c / l_c^2$, where v_c and l_c stand for the characteristic local fluid velocity and for a characteristic length of sheared fluid respectively, and the imposed pressure gradient of characteristic value $\Delta p_c / L_c$, where Δp_c is the characteristic pressure difference imposed along the characteristic macroscopic length L_c [24–26]

$$\frac{\Delta p_c}{L_c} \approx \frac{\eta v_c}{l_c^2}. \tag{7}$$

In this work, the well-posed boundary value problem (6) was solved with the FE code Comsol, using a mixed pressure–velocity formulation. Tetrahedrons were used in order to mesh the volume of interest, while linear and quadratic polynomial interpolations were, respectively, selected for the pressure fluctuation δp and the velocity fields $\underline{v}$ (P1–P2 elements). Fig. 6 presents a typical mesh used to run the simulations. Its main geometrical characteristic is to exhibit 2 elements in the lateral boundary air-gaps. The number of elements is about 15×10^3 and the corresponding number of degrees is 100×10^3. As revealed by a preliminary study, such a mesh allows to obtain sufficiently accurate results with reasonable computation time.

Hence, solving (6) for macroscopic pressure gradients oriented along three orthogonal axes and volume averaging the computed micro velocity field $\underline{v}$ leads to determine all the components of the permeability tensor. For example, by considering $\eta = 1$ Pa s and $\underline{\nabla}\bar{p} = -\underline{e}_1$, (5) gives $K_{1i} = \langle v_i \rangle$ ($i \in \{1,2,3\}$).

3.3. Qualitative analysis of mesoscopic velocity fields

Unless otherwise specified, the fabric that is considered is supposed to be made of a multitude of parallel stacked layers (3D periodicity). Slices representing typical computed velocity norm fields, are plotted in Fig. 7 when the imposed macroscopic unit pressure gradient equals $-\underline{e}_1$ and when the shear angle equals 0° (above) and 53° (below). Bright colours indicate regions where the flow intensity is large while dark ones regions where it is low. The various slice planes π_i are defined in Fig. 5b and f. Fig. 7 shows that the flow intensity is lower in the sheared case, which could corroborates with a permeability decrease (see next subsection). Whatever the shear angle, it also shows that flow occurs along two major channels. A similar noticing can be established when the imposed macroscopic unit pressure gradient is along $\underline{e}_2$. By contrast, when the pressure gradient is parallel to $\underline{e}_3$, flow follows four channels corresponding to the four holes between the yarns (see Fig. 5a, c and e).

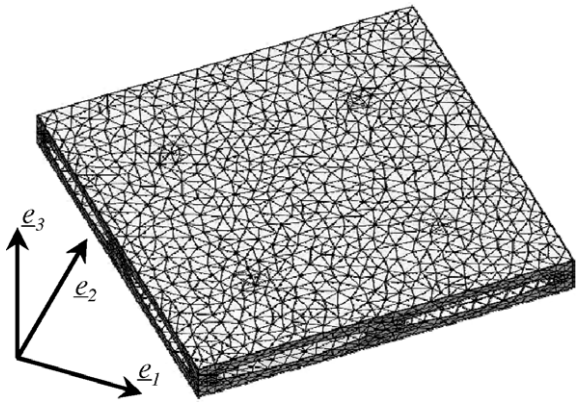

Fig. 6. Typical mesh of the fluid RVE in the non-deformed configuration.

3.4. Permeability

Fig. 8 represents the evolution of the components K_{11}, K_{22} and K_{33} of the corresponding permeability tensor $\underline{\underline{K}}$ expressed in the reference frame $\{\underline{e}_1, \underline{e}_1, \underline{e}_1\}$, as functions of the imposed shear angle. As shown in Fig. 5, $\underline{e}_1$ and $\underline{e}_2$ are aligned with rhombus diagonals while $\underline{e}_3$ indicates thickness direction. Fig. 8 brings up the following comments:

- The non-diagonal components (not shown in the figure) are found to be negligible with respect to the diagonal ones which means that the reference frame $\{\underline{e}_1, \underline{e}_1, \underline{e}_1\}$ is aligned with the principal axes of the permeability tensor.
- The in-plane permeability magnitude order (10^{-9} m^2) is realistic as compared with experimental results obtained using similar fabrics [7,9,27].

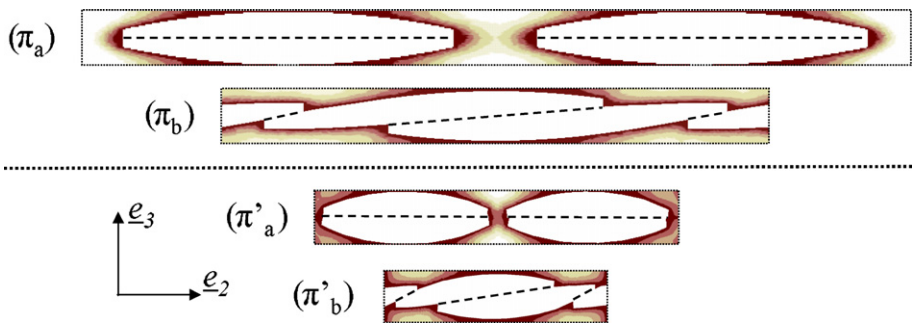

Fig. 7. Slices of velocity norm $\|\underline{v}\|$ along the planes π_a and π_b (see Fig. 5a) for the non-deformed configuration and along the planes π'_a and π'_b (see Fig. 5c) for the 53°-sheared configuration, when a unit macroscopic pressure gradient is imposed along the $\underline{e}_1$ axis (principal axis). Maximum in bright colour (=3×10^{-8} m s^{-1}) and minimum in dark colour (=0 m s^{-1}).

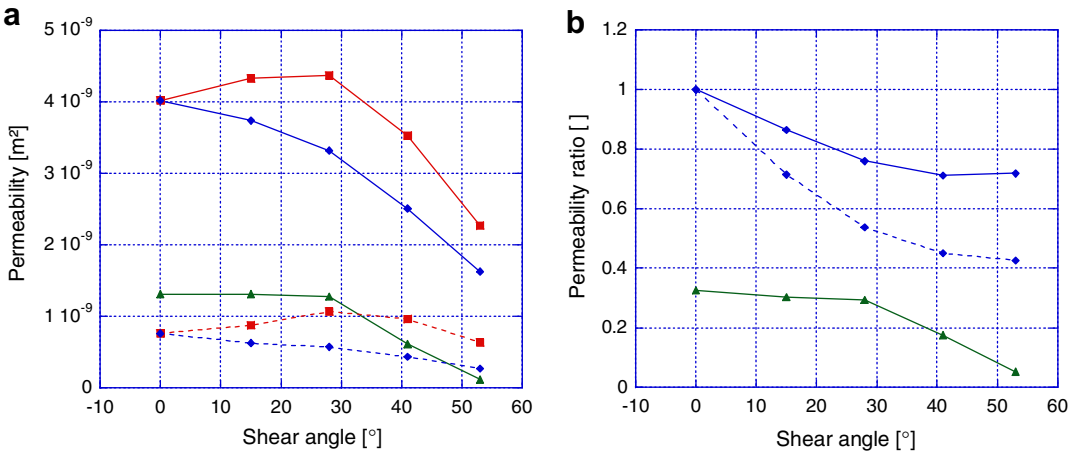

Fig. 8. (a) Computed permeabilities in the principal axes for different imposed shear angles. In continuous lines, a multi-layers configuration is considered while a single layer configuration is studied in dashed lines. ■: K_{11}; ♦: K_{22} and ▲: K_{33}. (b) Principal permeability ratios K_{22}/K_{11} (♦) and K_{33}/K_{11} (▲) for different imposed shear angles to the woven fabrics. In continuous lines, a multi-layers configuration is considered while dashed lines correspond to a single layer configuration.

- the non-deformed plain weave displays transverse isotropy ($K_{11} = K_{22} \neq K_{33}$). By contrast, as soon as it is sheared, it exhibits orthotropy ($K_{11} \neq K_{22} \neq K_{33}$).
- K_{22} undergoes a monotonous decrease with the shear angle. K_{11} increases and K_{33} is nearly constant for angles ranging from 0° to 30°. For larger shear angles, the two latter components decrease. By comparing permeabilities between the extreme configurations, K_{11} and K_{22} are found to decrease by a ratio 2 and K_{33} with a ratio 10. Notice that the trend recorded for K_{11} is experimentally retrieved by Smith et al. [4] who used plain-weave fabrics. Hammami et al. [3] performed experiments till 30° on JBMartin NCS fabric and also retrieved the same trend for K_{11} and for K_{22}. The complex trends emphasised in Fig. 8 are ascribed to changes of both the porosity (see Section 3.1) and the morphology of the plain weave during the shearing of the plain weave. Such changes are induced by two closely coupled deformation meso-mechanisms: the relative motions of tows and their intrinsic deformation. For instance, the drastic decrease of K_{33}, which is probably due to the locking of the holes perpendicular to the $\underline{e}_3$ direction, is induced both by the relative rotation of tows and their lateral crushing in the vicinities of contact zones (see Fig. 4).
- As suggested by Lai and Young [5], two relevant factors can be estimated, namely the ratio of principal permeabilities and the principal axis direction with respect to shear deformation of the fibre reinforcements (see Fig. 5). The relation between the principal axis direction β and the shear angle α is here obvious when considering symmetries of the considered warp and weft tows: $\beta = 45 + \alpha/2$. Conversely, the permeability ratio is not trivial, as depicted on Fig. 8b. The evolution of this factor with respect to the shear angle again highlights the loss of in-plane permeability isotropy when the fabric is sheared. We observe a decrease of K_{22}/K_{11} and K_{33}/K_{11}. This trend is also retrieved by Lai and Young [5] and Slade and Sozer [7].
- The in-plane principal permeabilities of a textile made of a single layer fabric have also been investigated. Results have also been plotted in Fig. 8. In that case, the upper and lower reinforcement sides were considered to face the mould faces, and a no slip condition was therefore imposed on the boundaries perpendicular to $\underline{e}_3$. As shown in Fig. 8a, the evolution of the in-plane permeabilities of a single mat with the shear angle follows the same trend as that observed for the multi-layers preform. However, they are five times smaller. Moreover, as depicted in Fig. 8b, shearing the single layer reinforcement induce stronger anisotropy than for the multi-layers one. Notice that Lai and Young [5] observed a decrease of the permeability when increasing the layer number. This apparent opposition could be due to the stacking sequence. Indeed, a perfectly parallel superposition is supposed in the present model, while an increase of the fibre volume fraction due to nesting effects is taken into account in the mentioned paper.

3.5. Mechanistic analysis of the results

In order to better understand the complex trends underlined in the previous subsection, it is possible to re-write, as suggested in previous studies [25,26], the macroscopic Darcy's law by accounting for both expression (7) and mesoscale flow patterns (cf. Section 3.3). This allows for instance to get rough estimates l_{ci} of the characteristic local length l_c when the macroscopic flow is along the principal direction $\underline{e}_i$ ($i \in \{1,2,3\}$). Indeed, for such situations, (7) can be re-casted as (no summation on the index i)

$$\frac{\partial \bar{p}}{\partial x_i} = -\frac{\eta}{l_{ci}^2} v_{ci}. \tag{8}$$

The characteristic local fluid flow velocity v_{ci} can also be linked with the macroscopic velocity $\langle \underline{v}_i \rangle$ by using a simple mass balance argument (no summation on the index i)

$$v_{ci} = \frac{S_{\mathrm{RVEi}}}{n_{ci} l_{ci}^2} \langle \underline{v}_i \rangle = \frac{1}{\phi_{ci}} \langle \underline{v}_i \rangle, \tag{9}$$

where S_{RVEi} represents the RVE area which is projected on a plane perpendicular to $\underline{e}_i$, n_{ci} the number of fluid channels mainly contributing to the flow (i.e. 2 for $i = 1,2$ and 4 for $i = 3$, cf. Section 3.3), and where ϕ_{ci} can be interpreted as a first estimation of the volume fraction of fluid (or pores) effectively involved in the flow. Hence, when combined with (5), the above relations allows us to write (no summation on the index i)

$$K_{ii} = \frac{n_{ci} l_{ci}^4}{S_{\mathrm{RVEi}}} = \phi_{ci} l_{ci}^2. \tag{10}$$

The last relation shows that K_{ii} closely depends on l_{ci} and ϕ_{ci}. The evolutions of l_{ci} and ϕ_{ci} with the shear angle have been displayed in the graph of Fig. 9 for the multi-layers preform. They have been determined from the knowledge of K_{ii} (cf. Section 3.4). This last graph reveals that the characteristic local lengths of sheared fluid

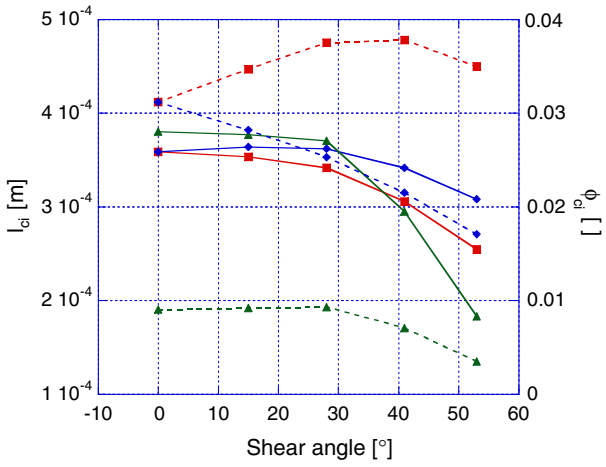

Fig. 9. Characteristic length l_c (continuous lines) and "active" porosity ϕ_c (dashed lines) in the three directions for different shear angles and for the multi-layers configuration. ■: $\underline{e}_1$ direction; ♦: $\underline{e}_2$ and ▲ $\underline{e}_3$.

l_{ci} constantly decrease with the shear angle. It also shows that the volume fractions of "active" pores ϕ_{ci} are much lower than the overall RVE porosity ϕ, and that the complex evolution of K_{11} may be ascribed to the complex trend recorded for ϕ_{c1}.

4. Concluding remarks

In this work, a method was proposed in order to compute the permeability of highly deformed woven fabrics. The method is divided in two steps. The first step consists in simulating the mesoscale pre-deformation of dry textile RVE's. Such calculations were carried out with a FE commercial code. A special attention was paid in order to limit simplifying assumptions that could induce biases on the deformed shape of solid RVE's. For example, the problem was solved within the framework of large geometrical transformations, and appropriate periodic boundary conditions were set to the external boundary of the solid RVE's. Likewise, yarn–yarn mechanical contacts were also taken into account in the simulations so that resulting deformed RVE's were kept consistent. Lastly, a realistic hypoelastic model was also used to better reproduce the intrinsic behaviour of yarns. This first step was applied to the in-plane shear of a symmetric glass plain weave. The macroscopic simulated response is in good accordance with experiment, and the shape of the deformed solid RVE seems realistic, even if further efforts are required to improve the quantitative validation of the simulated RVE deformed shapes. The second step consists in simulating the mesoscale flow through the as-deformed solid RVE's in order to compute the permeability tensor of the woven fabrics. Despite technical difficulties encountered to obtain suitable fluid RVE's from solid ones, this step could however be achieved with another commercial FE code. Numerical results have emphasised the drastic changes of the permeability tensor when the considered plain weave fabric was sheared: loss of transverse isotropy and non-trivial evolution of the components of the permeability tensor. Lastly, this work must be seen as a first preliminary study. Indeed, the above procedure could be applied and extended to other textiles and to other mechanical loadings textiles are usually subjected to (tension, biaxial tension, compression). Other types of flows as well as other physics could also be investigated: flow with non-negligible Reynolds numbers, flow of non-Newtonian fluids, flow through deformable woven fabric, thermal and solute dispersion, etc.

Acknowledgement

F. Loix would like to thank the CNRS for the research grant he had benefitted, as well as the Federation Rhône-Alpes Matériaux de Structures (FedeRAMS – CNRS) for its financial support.

References

[1] Abrate S. Resin flow in fibre preforms. Appl Mech RVE 2002;55:579–99.
[2] Rudd CD, Long AC, McGeehin P, Smith P. In-plane permeability determination for simulation of liquid composite molding of complex shapes. Polym Compos 1996;17:52–9.
[3] Hammami A, Trochu F, Gauvin R, Wirth S. Directional permeability measurement of deformed reinforcement. J Reinf Plast Compos 1996;15:552–62.
[4] Smith P, Rudd CD, Long AC. The effect of shear deformation on the processing and mechanical properties of aligned reinforcements. Compos Sci Technol 1997;57:327–44.
[5] Lai CL, Young WB. Model resin permeation of fibre reinforcements after shear deformation. Polym Compos 1997;18(5):642–8.
[6] Dungan FD, Senoguz MT, Sastry AM, Faillaci DA. On the use of Darcy permeability in sheared fabrics. J Reinf Plast Compos 1999;18:472–84.
[7] Slade J, Sozer EM, Advani SG. Fluid Impregnation of deformed preforms. J Reinf Plast Compos 2000;19:552–68.
[8] Heardman E, Lekakou C, Bader MG. In-plane permeability of sheared fabrics. Composite Part A 2001;32:933–40.
[9] Simacek P, Advani SG. Permeability model for a woven fabric. Polym Compos 1996;17(6):887–99.
[10] Dungan FD, Senoguz MT, Sastry AM, Faillici DA. Simulation and experiments on low-pressure permeation of fabrics: part I – 3D modeling of unbalanced fabric. J Compos Mater 2001;35:1250–83.
[11] Takano N, Zako M, Okazaki T, Terada K. Microstructure-based evaluation of the influence of woven architecture on permeability by asymptotic homogenization theroy. Compos Sci Technol 2002;62:1347–56.
[12] Laine B, Boust F, Boisse P, Hivet G, Lomov SV, Fanget A. Perméabilité des renforts fibreux. RVE Compos Matér Avancés 2005;15:385–400.
[13] Laine B, Hivet G, Boisse P, Boust F, Lomov SV. Permeability of the woven fabrics: a parametric study. In: Proceedings of the eighth ESAFORM conference, Cluj-Napoca; April 2005. p. 995–8.
[14] Lomov SV, Huysmans G, Luo Y, Parnas RS, Prodromou A, Verpoest I, et al. Textile composites: modelling strategies. Composite Part A 2001;32:1379–94.
[15] Hivet G, Boisse P. Consistent 3D geometrical model of fabric elementary cell. Application to a meshing preprocessor for 3D finite element analysis. Finite Elem Anal Des 2005;42:25–49.
[16] Boisse P, Zouari B, Daniel J-L. Importance of in-plane shear rigidity in finite element analyses of woven fabric composite forming. Composite Part A 2006;37:2201–12.
[17] Badel P, Vidal-Sallé E, Boisse P. Computational determination of in-plane shear mechanical behaviour of textile composite reinforcements. Comput Mater Sci 2007;40(4):439–48.
[18] Hughes TJR, Winget J. Finite rotation effects in numerical integration of rate constitutive equations arising in large deformation analysis. Int J Num Methods Eng 1980;15:1862–7.
[19] Crisfield MA. Non linear analysis of solids and structures. Advanced topics, vol. 2. Chichester: Wiley; 1997.
[20] Gasser A, Boisse P, Hanklar S. Mechanical behaviour of dry fabric reinforcements, 3D simulations versus biaxial tests. Comput Mater Sci 2000;17:7–20.
[21] Cao J, Cheng HS, Yu TX, Zhu B, Tao XM, Lomov SV, et al. A cooperative benchmark effort on testing of woven composites. In: Proceedings of the seventh international ESAFORM conference on material forming, Trondheim, Norway; 2004. p. 305–8.
[22] Auriault J-L, Boutin C. Deformable porous media with double porosity. Quasi-statics: I coupling effects. Transp Porous Media 1992;7:63–82.
[23] Nedanov PB, Advani SG. Numerical computation of the fibre preform permeability tensor by the homgenization method. Polym Compos 2002;23:758–70.
[24] Auriault J-L. Heterogeneous medium. Is an equivalent macroscopic description possible? Int J Eng Sci 1991;29:785–95.
[25] Orgéas L, Idris Z, Geindreau C, Auriault J-L, Bloch J-F. Modelling the flowof power-lawf luids through anisotropic porous media at low-pore Reynolds number. Chem Eng Sci 2006;61:4490–502.
[26] Orgéas L, Geindreau C, Auriault J-L, Bloch J-F. Upscaling the flow of generalised Newtonian fluids through anisotropic porous media. J Non-Newtonian Fluid Mech 2007;145:15–29.
[27] Belov EB, Lomov SV, Verpoest I, Peters T, Roose D, Parnas RS, et al. Modelling of permeability of textile reinforcements: lattice Boltzmann method. Compos Sci Technol 2004;64:1069–80.